Chapter 6: **OPTICAL CHARACTERISATION OF THE MATRIX**

It is interesting for later applications to determine the spectroscopic properties of lanthanide ions in RTP:Nb crystals. However, it is essential for the subsequent development of these materials to fully characterise the matrix in which these ions are hosted. In this chapter we study the optical properties of RTP:Nb crystals for their later application as laser materials. We compare all the properties measured to those of RTP because in most cases, RTP:Nb crystals are better than RTP crystals for self-frequency doubling laser applications when doped with Ln^{3+} ions.

6.1. Measurements of the refractive indexes of $RbTiOPO_4$ and $RbTiOPO_4$:Nb crystals in the three principal directions.

We need accurate measurements of the refractive indexes of a non-linear optical material to accurately predict the phase-matching directions and the spectral bandwidth acceptances.

Figure 1 in *paper IV* shows the chromatic dispersion curves of $RbTi_{1-x}Nb_xOPO_4$ (x = 0 and 0.06) for the three principal directions (x = ***a***; y = ***b***; z = ***c***) in the visible and near-IR spectral regions. The results for RTP agree well with those in the literature.[208] However, there were significant changes in the three indexes of RTP:Nb with respect to RTP. Although n_x practically did not change, n_y and n_z increased significantly in RTP:Nb crystals. This implies that, as with KTP:Nb crystals,[102] the birefringence of RTP:Nb crystals is higher than that of the RTP crystals.

We fitted these results with a Sellmeier equation using one UV pole and an IR correction term:

$$n^2 = A + \frac{B\lambda^2}{\lambda^2 - C} - D\lambda^2 \qquad \text{Eq. 6.1}$$

Table 6.1 shows the Sellmeier coefficients obtained for RTP and RTP:Nb crystals at room temperature calculated with the refractive indexes measured in the range of between 0.450 and 1.500 μm.

Table 6.1. *Sellmeier coefficients for $RbTi_{1-x}Nb_xOPO_4$ (x = 0 and 0.06).*

Principal refractive indexes	A	B	C μm^2	D μm^{-2}	$\partial n/\partial T$ K^{-1}
$RbTiOPO_4$					
n_x	1.6795	1.4281	0.0325	0.0119	5.6×10^{-5}
n_y	2.0360	1.0883	0.0437	0.0090	9.1×10^{-5}
n_z	2.2864	1.1280	0.0562	0.0188	6.6×10^{-5}
$RbTi_{0.94}Nb_{0.06}OPO_4$					
n_x	2.4753	0.6664	0.0578	0.0180	4.7×10^{-5}
n_y	1.1320	2.0885	0.0278	0.0096	7.7×10^{-5}
n_z	2.2619	1.2069	0.0594	0.0168	9.2×10^{-5}

We also studied how the refractive indexes change with temperature in the 293-473 K range. Table 6.1 also shows the thermo-optic coefficients estimated at λ = 632.8 nm. As we can see, the thermo-optic coefficients of RTP and RTP:Nb crystals are very similar: $\partial n_x/\partial T$ and $\partial n_y/\partial T$ are slightly

smaller and $\partial n_z/\partial T$ is slightly greater in RTP:Nb than in RTP. However, the changes in the refractive indexes as the temperature changes are so small that they practically do not affect the phase-matching directions in the operating crystal.

6.2. The transparency window of $RbTiOPO_4$ and $RbTiOPO_4$:Nb crystals.

It is important for both research and device engineering to know the crystal transmission. Generally, the transparency for KTP isomorphs starts at a wavelength of approximately 0.35 μm and ends at 4.5 μm for the phosphate compounds in bulk crystals. However, the anisotropic nature of these materials yields three different transmission spectra, depending on the polarisation of the transmitted beam. In this Section we present measurements of polarised optical transmission in RTP and RTP:Nb crystals over the full transmission window in both materials at room temperature.

We took these measurements with the ***b***- and ***c***- crystal axes oriented parallel to the electrical field of the measurement beam in very thin crystals (of the order of microns) perpendicular to the ***a***-axis. We took special care to resolve transmission differences between polarisation directions at the ultraviolet (UV) absorption edge. The measurements with the FTIR spectrometer were taken without polariser at room temperature in N_2 to avoid the absorption of atmosphere water vapour.

Absorption bands near the UV absorption edge of the crystals can affect the optical transparency of the crystals. In KTP crystals, the appearance of these bands is related to an increase in susceptibility to optical damage due to doping ions.[209,210] In as-grown RTP:Nb crystals, broad bands in the visible region were observed (see Figure 6.1 (a)) before annealing. If we compare the results obtained with those obtained in optical damaged KTP or in KTP samples reduced with H_2,[211] we find that these bands, centred at 594 and 639 nm, may be related to the presence of Ti^{3+}, because we can assign the two peaks to this ion.[212] When the sample was annealed at 773 K for 3 hours in ambient atmosphere, these broad absorption bands disappeared (see Figure 6.1 (b)). The existence of these bands corresponding to Ti^{3+} is therefore further proof of the electrical charge self-compensation in this family of compounds, in addition to the creation of Rb-vacancies (see Chapter 4). Also the existence of Ti^{3+} in the as-grown crystals could explain why we could not find a logical relationship between the concentration of Nb^{5+} in the crystals and the creation of Rb-vacancies.

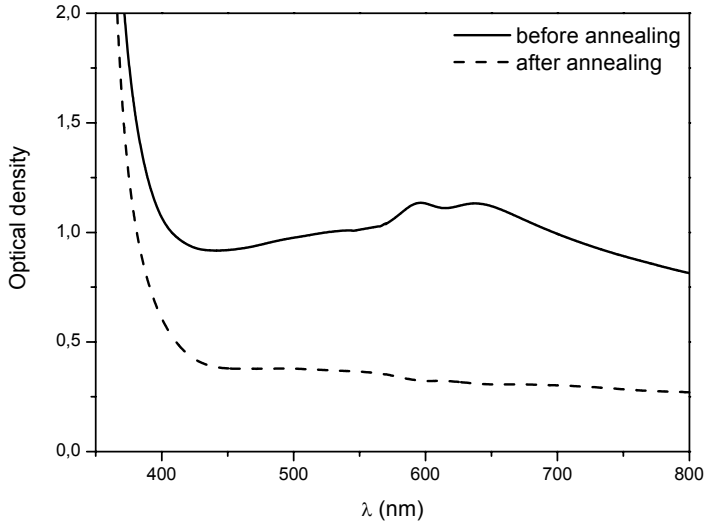

Figure 6.1. *Absorption spectra of an as-grown $RbTi_{0.97}Nb_{0.03}OPO_4$ crystal before annealing and after annealing measured at room temperature.*

Figure 6.2 shows a low-resolution overview of the window in the respective crystals for polarisation parallel *E//z*. Common features of these crystals were high transparency from 0.6 to 4.2 μm and a sharp UV absorption edge at approximately 0.35 μm. The slope of the IR multiphonon absorption edge declined slowly over approximately 5 μm, with broadband absorption lines in the centre of the slope. The main differences in transmission between crystal isomorphs were in the UV-to-visible wavelength range and at the OH absorption lines near 2.8 μm.[177]

The maximum values of transparency and the wavelengths of the UV absorption edge among the various crystal types and polarisations were different. Figure 6.3 shows the typical RTP and RTP:Nb transmission spectra on the UV absorption edge for the *E//y* and *E//z* polarisation directions from 0.6 μm to the UV absorption edge in the ultraviolet region. The UV absorption edge is generally attributed to the absorption of the Ti-O subgroup.[213] Table 6.2 lists the values of UV absorption edge for these samples. This is defined as the wavelength at which the transparency has decreased by an *e*-factor of its maximum value. By comparing with KTP,[177] we expected the shortest value of UV absorption edge to be for *E//x* and the longest value to be for *E//z*, but, because of the samples we used had a particular habit as we explained in Chapter 4, we could only analyse the *E//y* and *E//z* configurations. The UV absorption edge is a function of polarisation and Nb content, and shifted to longer wavelengths when the spectra were collected parallel to the *z*-axis and when Nb was present in the crystals. We can see the variation in the UV absorption edge between RTP and RTP:Nb crystals more easily if we study the absorption coefficient (α) instead of the transmission (see Figure 3 in *paper II* and Figure 2 in *paper IV*). Also, the slope of the curve was lower when Nb was present in the crystal.

Note that the UV absorption edge of RTP was clearly shorter than that reported by Hansson et al.[177] because the quality of our sample was higher.

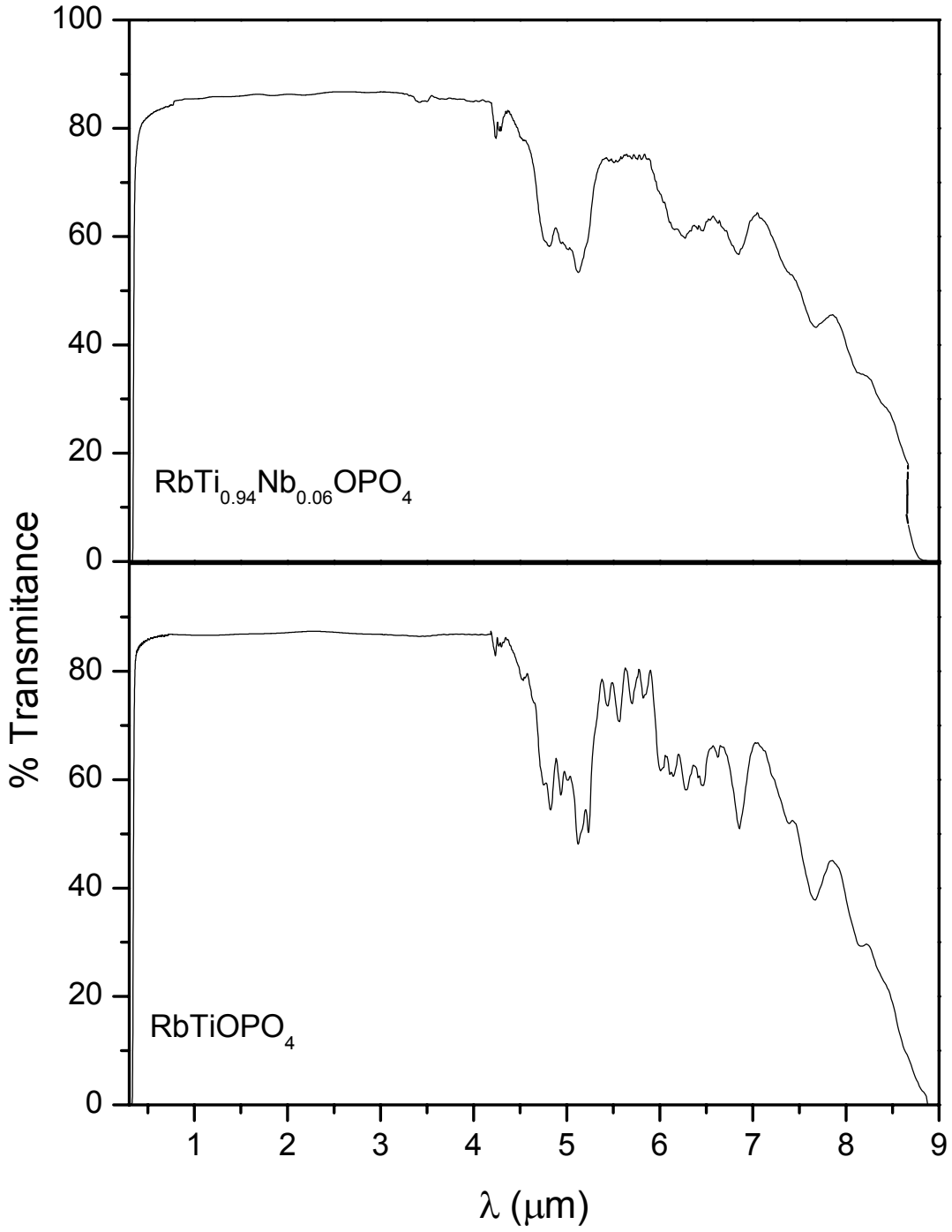

Figure 6.2. *Transparency windows of (a) $RbTiOPO_4$ crystal and (b) $RbTi_{0.94}Nb_{0.06}OPO_4$ crystal.*

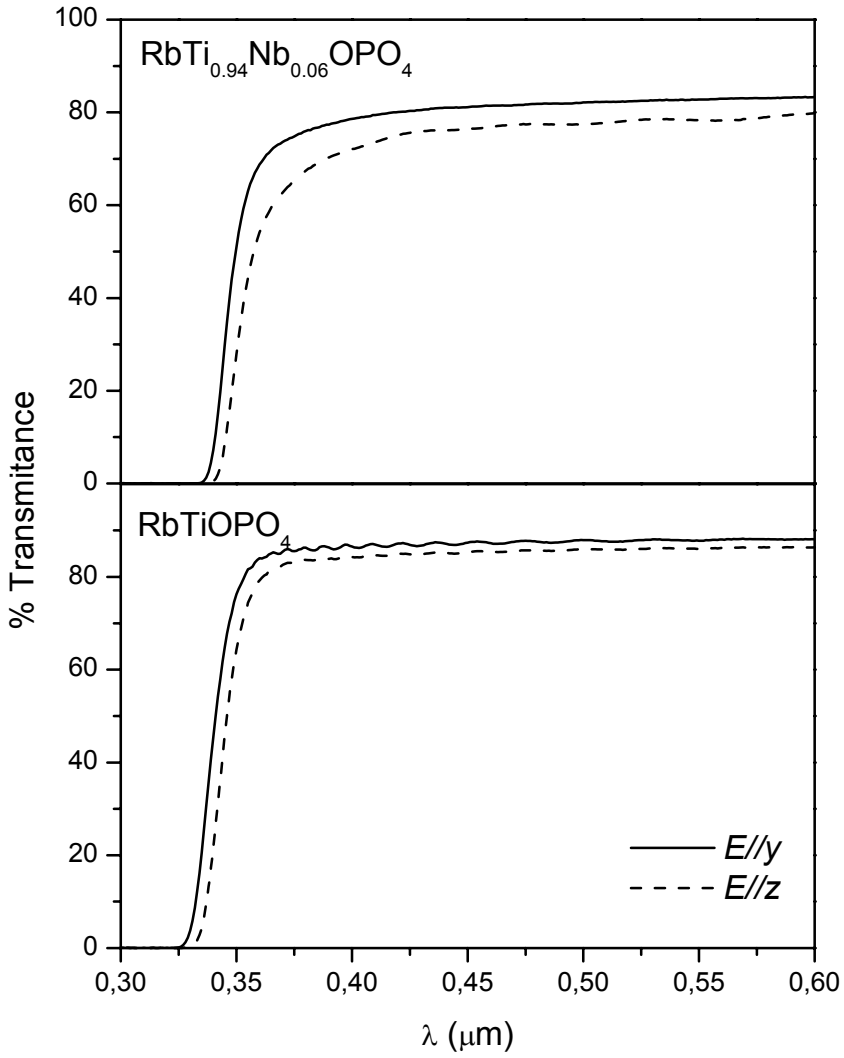

Figure 6.3. *Polarised transmission spectra on the UV absorption edge for $RbTi1_{-x}Nb_xOPO_4$ (x = 0 and 0.06).*

The transparency was always maximum for spectra collected with polarised light parallel to the *y*-axis. Also, by comparison with KTP,[177] we expected maximum transparency for the spectra collected parallel to the *x*-axis, but we could not perform this analysis. The difference in transparency between the spectra collected parallel to the *y*-axis and the spectra collected parallel to the *z*-axis was around 3-4%, depending on whether the sample contained Nb or not. We also found that this maximum value is a function of the concentration of Nb: maximum transparency was 5 % lower in the sample containing Nb.

As we were looking for type-II birefringent phase-matching at around 1 μm in the family of KTP, propagation in the *x*-*y* plane provided the large effective non-linearity, and the second harmonic wavelength was also polarised *E//z*. The birefringent phase-matching directions for these crystals was not yet established (see Section 6.4 in this Chapter), but Table 6.2 also includes the values of

transmission in *y* polarisation at the non-critical phase-matching wavelengths for both crystals and their corresponding SHG wavelengths. Both fundamental and SHG wavelengths are in the high-transmission region of the transparency window. The low differences in transmission are good for avoiding thermal dephasing of the conversion process in high-power SHG, particularly for quasi-phase-matching applications.

Table 6.2. *UV absorption edges and values of transmission at the non-critical phase-matching directions for* $RbTi_{1-x}Nb_xOPO_4$ *(x = 0 and 0.06).*

Crystal	**E//y**	**E//z**	**Transmission at fundamental**	**Transmission at SHG**
$RbTiOPO_4$	338	342	89.0 %	87.6 %
$RbTi_{0.94}Nb_{0.06}OPO_4$	345	350	85.8 %	81.9 %

The intermanifold electron transitions of the lanthanides can be strongly coupled with the lattice vibrations. It is important to know the phonon frequencies in order to interpret the substructure in the absorption and fluorescence spectra of these ions and identify the mid-IR cut-off edge.

Transmission on the IR side of the spectra in these crystals depended on the propagation length of the sample (see Figure 6.4 for pure RTP), which is the same behaviour showed previously for KTP.[214] The IR absorption edge in these crystals is caused by the first and second overtones of the ν_3 and ν_1 fundamental vibrations of the phosphate ion in the tetrahedra.[215] The higher the thickness of the sample, the greater the concentration of the phosphates with which the incident light can interact, and the higher the intensity of the ν_3 band. When this concentration is high enough, this band can close the transparency window in the IR region at around 4.5 μm. If the sample is thin enough so as not to allow the ν_3 bands to close the transparency window, this window can extend to around 9 μm. This behaviour must be taken into account when these crystals are used as thin films, such as in applications derived from epitaxial growth,[216,217] where additional interactions of the light in the IR region of the spectra can be developed.

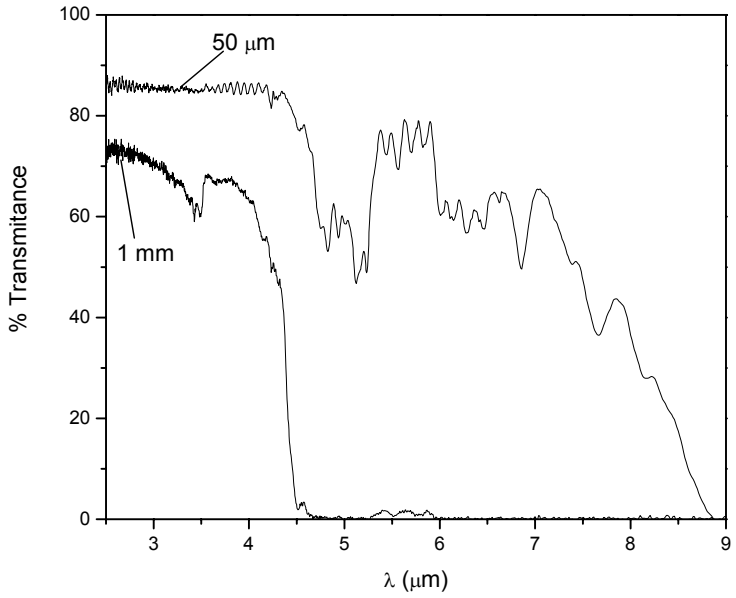

Figure 6.4. *IR transmission of an $RbTiOPO_4$ crystal as a function of its thickness.*

RTP and RTP:Nb crystals belong to the point group of symmetry mm2 and show 192 vibrational degrees of freedom. At zero wavevector, the irreducible representations of the vibrational optic phonon modes in this point group are the following:

$$\Gamma_{vib} = 47\ A_1 + 48\ A_2 + 47\ B_1 + 47\ B_2 \qquad \text{(Eq. 6.2)}$$

One A_1, one B_1 and one A_2 modes are acoustic and the rest are optical modes. A_1, B_1 and B_2 are IR active with dipole moments oriented along the *z*, *x* and *y* directions, respectively, and all of them are Raman active.

The free phosphate group belongs to the $\bar{4}3m$ point group of symmetry with 9 internal modes of vibration. This can be described as two bond stretching vibrations (ν_1 and ν_3) and two distorting vibrations (ν_2 and ν_4). The vibrational modes of a perfect *isolated* TiO_6 octahedron can be decomposed into two pure bond stretching vibrations (ν_1 and ν_2), two inter-bond angle-bending vibrations (ν_5 and ν_6) and two combinations of stretching and bending vibrations (ν_3 and ν_4). Although some of these vibrational modes are not IR-active in the perfect tetrahedron or octahedron, the distortion of these polyhedra in the RTP structure breaks the selection rules and all the vibrational modes can be seen in IR.

Figure 6.5 shows IR unpolarised band-edge transmission from 2.6 to 9.0 μm for all crystals. The slopes were similar for all samples, and there was no band shifting. As the principal bands in this region are caused by vibrations of the PO_4 tetrahedra, this is another proof that Nb only substitutes Ti in the structure. Table 6.3 shows the assignation of the IR bands observed in $RbTi_{1-x}Nb_xOPO_4$ (x = 0, and

0.06) crystals. The reduction in the symmetry of the phosphate group breaks the degeneracy associated to the ν_3 vibration, and at least six bands were observed. In all cases, these bands were centred at shorter wavenumbers than with KTP.[213]

There were significant differences in the presence of bands attributed to OH^- in the samples with Nb and in samples without Nb. These bands were not present in the pure RTP sample, but a band corresponding to this ion appeared at 2.6 μm (3810cm^{-1}) in the sample containing Nb. These OH^- bands were attributed to the adsorption of environment water by the crystal. They are found in multiple positions in each of the different structural oxygens in the structure of RTP. These results seem to indicate that RTP:Nb crystals are a little more hygroscopic than pure RTP crystals, but the intensity of the OH^- band is lower than that reported by Hansson et al. in crystals of the KTP family.[177]

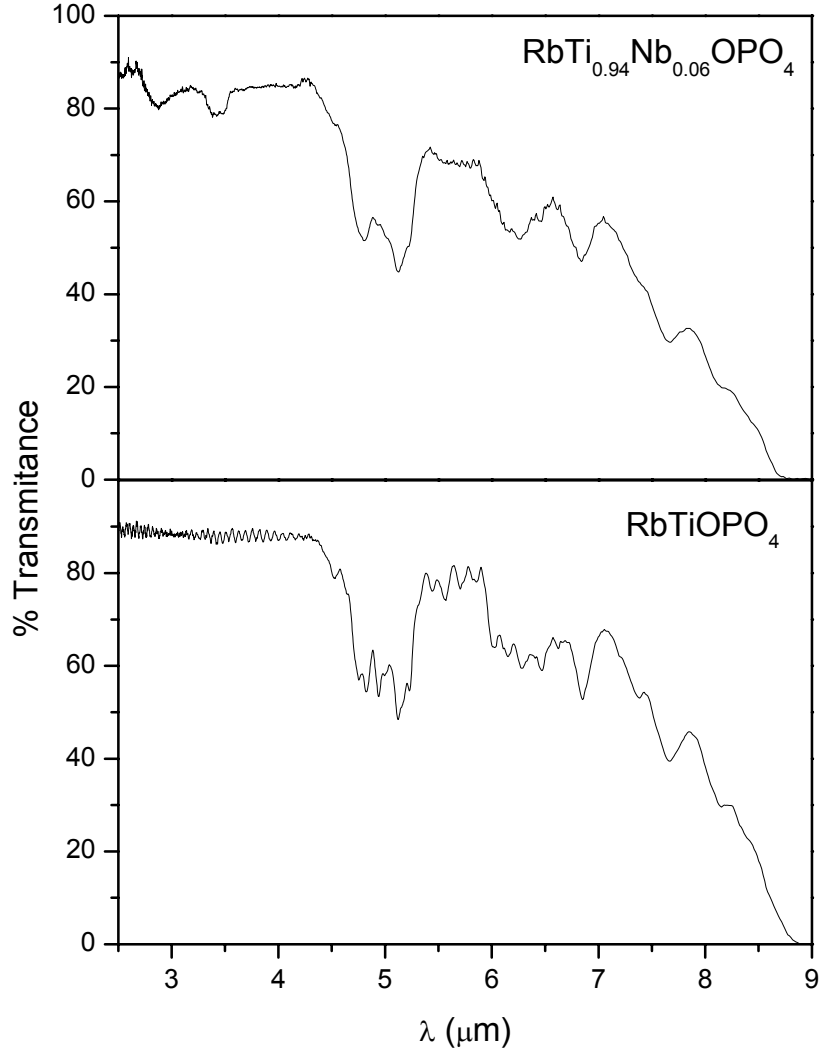

Figure 6.5. *IR unpolarised band-edge transmission for $RbTi_{1-x}Nb_xOPO_4$ (x = 0 and 0.06).*

Table 6.3. *IR bands observed in $RbTi_{1-x}Nb_xOPO_4$ (x = 0 and 0.06) crystals.*

$RbTiOPO_4$	$RbTi_{0.94}Nb_{0.06}OPO_4$	Assignation
	3810	Tensions of H_2O with H-bonds
	3475	
	2987	Second overtone ν_3 PO_4
	2956	
	2928	
	2860	
2361	2361	
2341	2341	
2324	2327	
2210	2210	
2153		First overtone ν_3 PO_4
2102		
	2098	
	2078	
2071		
2026	2026	
1996	1996	
1952	1952	
1907	1907	
1835	1835	
	1815	
	1801	
1798		
	1788	
	1778	
	1767	
	1757	
1754		
1741		
	1737	
	1726	
1719		
1709		
	1706	
1690	1690	
1665		Combination bands $\nu_3 + \nu_4$ PO_4
	1656	
	1642	
1637		
1627		
	1623	
	1597	
1593		
	1579	
1576		
	1562	
1559		
1549	1549	
1511	1511	
1494	1494	
1463	1463	
1353	1353	
1306	1306	Combination bands $\nu_1 + \nu_2$ PO_4
1227	1227	

6.3. A comparative Raman study of $RbTiOPO_4$ and $RbTiOPO_4$:Nb crystals.

A short study of polarised Raman scattering of RTP was included in the extensive polarised Raman scattering study of KTP,[194] but detailed information about its phonon frequencies has not yet been published. In this Section we analyse in detail the spontaneous Raman scattering for RTP and RTP:Nb crystals.

Two samples of $RbTi_{1-x}Nb_xOPO_4$ (x = 0 and 0.06) of a thickness of around 2 mm in each direction were cut and polished perpendicular to the three principal axes *x*, *y* and *z*. Figure 6.6 shows the Raman unpolarised spectra recorded at room temperature in the 20 to 1200 cm^{-1} frequency range for these crystals. The structure of the spectra is complicated, with about 100 peaks of very different intensities. The two strongest structures appear around 280 cm^{-1} and 700 cm^{-1}, which could, like with KTP,[194] make these crystals excellent candidates for stimulated Raman converters or oscillators. Several peaks of intermediate intensity are seen at 204, 330, 370 and 635 cm^{-1}. As is normally expected from the complex crystallographic structure, many additional lines of lower intensity are detected within the whole frequency range, and especially below 250 cm^{-1}. There is a general broadening of the lines in RTP:Nb crystals, which indicates that the structure is not homogeneous.[218]

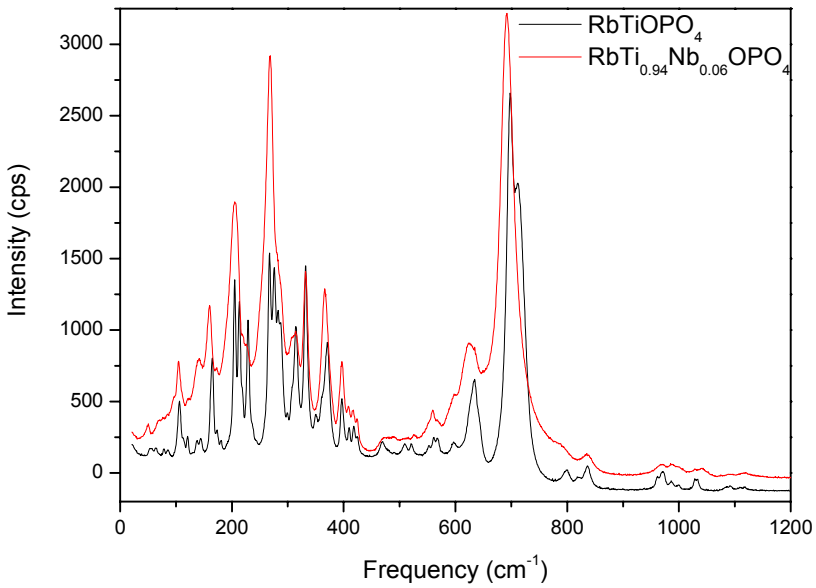

Figure 6.6. *Unpolarised Raman spectra recorded in $RbTi_{1-x}Nb_xOPO_4$ (x = 0 and 0.06) at room temperature.*

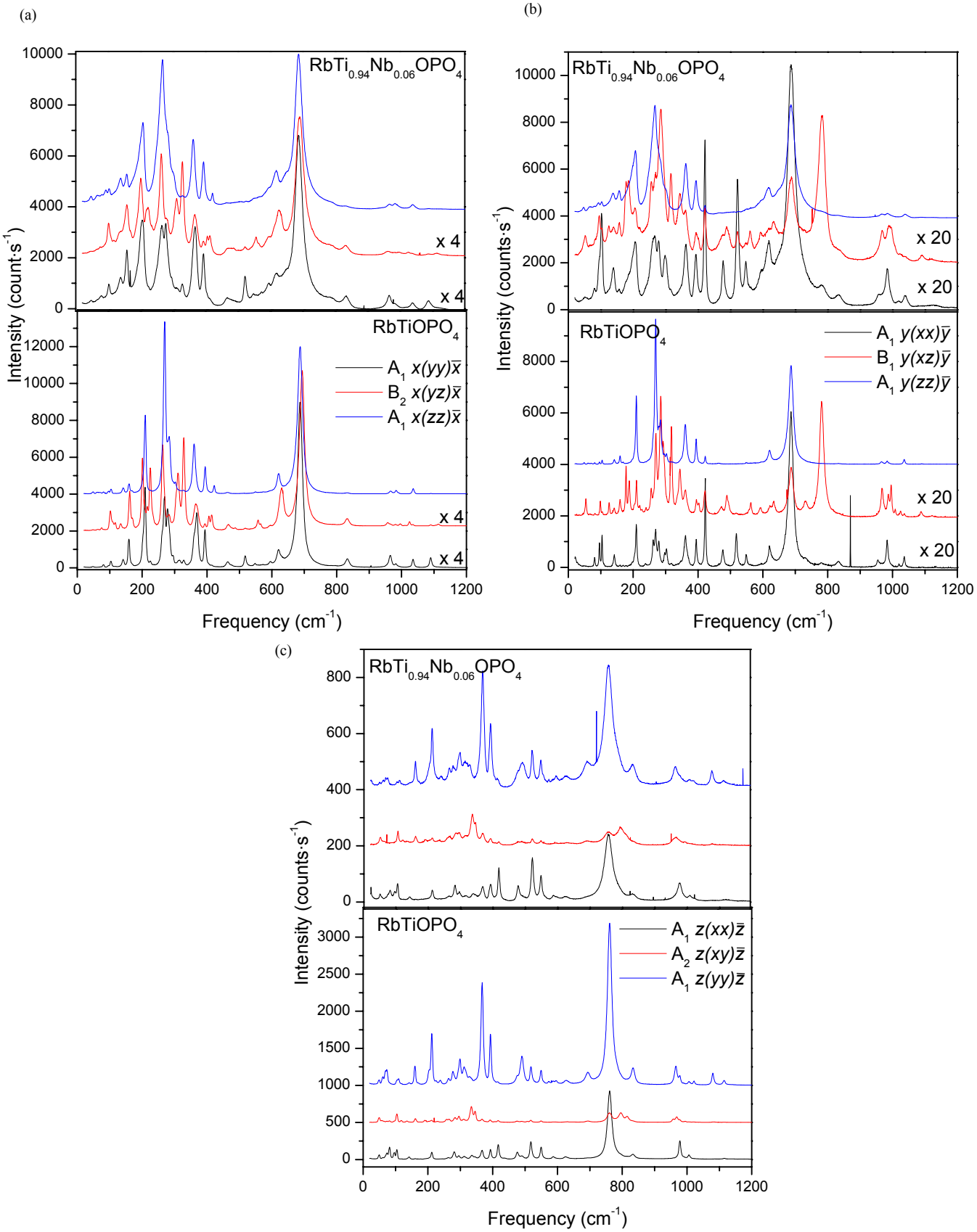

Figure 6.7. *Raman spectra of recorded in $RbTi_{1-x}Nb_xOPO_4$ ($x = 0$ and 0.06) at room temperature in the back-scattering geometry for the (a) $x(yy)\bar{x}$, $x(yz)\bar{x}$, $x(zz)\bar{x}$ configurations, (b) $y(xx)\bar{y}$, $y(xz)\bar{y}$, $y(zz)\bar{y}$ configurations and (c) $z(xx)\bar{z}$, $z(xy)\bar{z}$, $z(yy)\bar{z}$ configurations.*

Figure 6.7(a) shows the polarised spectra belonging to the $x(yy)\bar{x}$, $x(yz)\bar{x}$, and $x(zz)\bar{x}$ scattering configurations, corresponding to the A_1, B_2 and A_1 symmetry representations, respectively, and involving phonons propagating along the [100] direction. Figure 6.7 (b) shows the polarised spectra belonging to the $y(xx)\bar{y}$, $y(xz)\bar{y}$, and $y(zz)\bar{y}$ scattering configurations, corresponding to the A_1, B_1 and A_1 symmetry representations and involving phonons propagating along the [010] direction. Finally, Figure 6.7(c) shows the polarised spectra belonging to the $z(xx)\bar{z}$, $z(xy)\bar{z}$, and $z(yy)\bar{z}$ scattering configurations, corresponding to A_1, A_2 and A_1 symmetry representations, respectively and involving phonons propagating along the [001] direction. The $x(zy)\bar{x}$, $y(zx)\bar{y}$, and $z(yx)\bar{z}$ configurations are not shown because they are equivalent to the $x(yz)\bar{x}$, $y(xz)\bar{y}$, and $z(xy)\bar{z}$ configurations. We only recorded them to confirm the sample orientation. Tables 6.4, 6.5 and 6.6 show the principal modes of RTP and RTP:Nb as derived from our measurements and their assignment in the various configurations.

The large modifications of the Raman spectra observed for several geometrical configurations as well as several propagation directions of the phonons were possible because of the single-crystal nature of our crystals. All the spectra of A_1 symmetry produce slightly different results. These differences may have been due to a strong anisotropy in the phonon dispersion and to the fact that the experiment reached, with different geometrical conditions, scattering from phonons with different polarisations. In the case of phonons propagating along the [100] and [010] directions, the *zz* susceptibility of the A_1 symmetry species was clearly higher than the *xx* and the *yy* susceptibilities. In the case of phonons propagating along the [001] direction, the *yy* susceptibility was higher than the *xx* susceptibility. The intensity of the B_2 symmetry species was similar to that of A_1 in the $x(yy)\bar{x}$ configuration, the intensity of the B_1 symmetry species was similar to that of A_1 in the $y(xx)\bar{y}$ configuration and the intensity of the A_2 symmetry species was the lowest of all configurations. Generally, the spectra corresponding to RTP are more intense than the spectra corresponding to RTP:Nb. In RTP, the most intense configuration was the one that corresponded to phonons propagating along the [100] direction. The next most intense configuration corresponded to phonons propagating along the [010] direction, and the lowest intensity was for phonons propagating along the [001] direction. In RTP:Nb crystals, however, intensity was highest for phonons propagating along the [010] direction and lowest for phonons propagating along the [001] direction. The small frequency shifts, which are observed for similar groups of phonons in the different polarisations of the same crystal, may be caused by the possibility of detecting modes of mixed polarisation character in Raman scattering.

By comparing the Raman spectra of RTP and RTP:Nb crystals, we can distinguish between modes involving mostly the TiO_6 group and modes involving mostly the PO_4 or Rb^+ groups, because Nb substitutes Ti in the structure.

The fully symmetric ν_1 vibration of PO_4 was observed at around 833 cm^{-1}. This vibration, which was not seen in the $y(xx)\bar{y}$ and $y(xz)\bar{y}$ configurations, was very strong in the $z(yy)\bar{z}$ configuration, but was weaker for the other configurations. Such behaviour is typical of totally symmetrical stretching vibrations in PO_4.[219] Also, the fact that at least two lines can be attributed to this mode, indicates that there were different structural positions of P in the framework. The ν_2 mode appeared as 2 peaks, one centred at around 390 cm^{-1} or 420 cm^{-1} depending on the configuration. The ν_3 and ν_4 triply degenerate modes were located between 1000 and 1100 cm^{-1} for ν_3 and between 450 and 575 cm^{-1} for ν_4. The antisymmetrical stretching mode ν_3 did not have such a strong polar character as ν_1 and was easily seen in practically all configurations.[220] These peaks do not normally shift when Nb is incorporated in the crystal. This happens mainly with ν_1 and ν_2 vibrations. However, with ν_3 and ν_4, some band shifting of between 2 and 4 cm^{-1} to longer wavenumbers was observed when Nb was present in the crystals. This shifting could not be related to the substitution of P by Nb since shifting to shorter wavenumbers was expected in that case because Nb is heavier than P.

The most intense structures, located around 202, 265 and 696 cm^{-1}, arose from vibrations involving the TiO_6 octahedra, as was confirmed by the general shift of these bands in crystals containing Nb. We expected the ν_1 mode to be the most intense of the high-frequency modes. The intense broadband around 696 cm^{-1} was related to this mode and had a doublet character in pure RTP. This could be due to a splitting into a planar mode and an axial mode that is compatible with the pseudo-tetragonal symmetry with respect to the Ti-O bond distances. It may also be due to the fact that the ν_3 stretching mode involving a Ti-O anti-phase motion probably had energy in the region of 700 cm^{-1}. As no bands could definitely be attributed to ν_3, we think that the most likely reason is the second one. The high intensity of the band associated with ν_1 indicates a high ordered structure. As the intensity is maintained in the case of the RTP:Nb crystal the non-homogeneity observed by the broadening of the bands, did not affect the order of the structure.[221] The ν_2 mode occurred at a lower energy and corresponded to the weaker line at 632 cm^{-1}. The ν_5 Raman mode, which was expected to be intense, was detected at 265 cm^{-1}. The ν_4 mode appeared as a doublet structure with peaks at 313 or 329 cm^{-1} depending strongly on the polarisation studied. The shortest frequencies were obtained for phonons propagating along the [010] direction, for which the apical oxygens of the $Ti(1)O_6$ octahedra were oriented in the same direction, which propitiated the ν_4 vibrational mode. The largest frequencies were obtained for phonons propagating along the [100] direction, for which the apical oxygens of the $Ti(2)O_6$ octahedra were oriented in the same direction, which again propitiated the ν_4 vibrational mode. The fact that the mean Ti-O bond was longer in $Ti(2)O_6$ than in $Ti(1)O_6$ (see Chapter 4) could be responsible for the different frequencies of vibration of this mode, as it was observed in other compounds made up of octahedra of transition metals.[219] The intensity of this mode for photons

propagating along the [001] direction was so low because no octahedra were located in a suitable orientation for this vibration. Finally, the line near 205 cm^{-1} belongs to the ν_6 mode, which was activated by the distortion of the TiO_6 group and the low site symmetry C_1. This vibration mode appeared as a triplet with main peaks at 202, 212 and 227 cm^{-1}. Additional bands at 359 and 365 cm^{-1} in RTP and RTP:Nb crystals, respectively, can be attributed to the existence of TiO_6 and NbO_6 groups, sharing corners.[222] Also, the band appearing as a shoulder at 788 cm^{-1} in the RTP:Nb samples was assigned to the vibration of the Nb-O-Ti group, which indicates that Ti was substituted by Nb. The absence of a band corresponding to NbO_4 groups reinforces the fact that Nb ions only substituted Ti in the structure. All these bands tended to shift to shorter wavenumbers (between 2 and 4 cm^{-1}) when Nb is present in the crystals. This was as expected when Ti is substituted by a heavier ion such as Nb.

The intensity ratio $I_{\upsilon 2}/I_{\upsilon 1}$ is a measure of the distortion of the octahedra. In unpolarised spectra, these intensities are more different in RTP crystals than in RTP:Nb crystals, which confirms that the distortion of the octahedra is more similar in RTP:Nb crystals than in RTP crystals.

If we base our study on the previous study of Kugel et al.,[194] it seems reasonable to complete the internal mode picture with an analysis involving collective and coupled mode propagation of the crystal lattice. The structures lying between 150 and 200 cm^{-1} consist of a vibration in which the whole octahedron is displaced relative to the lattice. This is confirmed by the shifting of these bands when Nb was present in the crystals. Other bands involving polar vibrations between Rb^+ and the neighbouring oxygens ions were seen at around 90 cm^{-1}, and the metal-metal vibrations were seen at around 110 cm^{-1}. Finally, the translational modes associated to Rb^+ were seen at around 140 cm^{-1}. The low frequency of the external lattice modes involving Rb^+ below 200 cm^{-1} shows the weakness of the bonds between Rb and the neighbouring ions, which are essentially ionic.[219]

Despite the consistency of these assignments, made by comparison with KTP, such a description is a first approach to understand the vibrations of RTP and how they are affected by the presence of dopants in the crystal.

Table 6.4. *Raman bands observed in $RbTi_{1-x}Nb_xOPO_4$ (x = 0 and 0.06) at room temperature for the $x(yy)\bar{x}$, $x(yz)\bar{x}$, $x(zz)\bar{x}$ configurations.*

$RbTiOPO_4$			**$RbTi_{0.94}Nb_{0.06}OPO_4$**			**Assignation**
$x(yy)\bar{x}$	$x(yz)\bar{x}$	$x(zz)\bar{x}$	$x(yy)\bar{x}$	$x(yz)\bar{x}$	$x(zz)\bar{x}$	
			47 vs	47 vs	47 vs	
50 vs		50 vs				
	62 vs	62 vs				
			67 vs	67 vs	67 vs	
		70 vs				
	76 vs		76 vs	76 vs		
81 vs		81 vs			81 vs	Polar vibrations Rb-O
					93 vs	
97 vs		97 vs				
			102 s	102 m		
105 s	105 s	105 vs			105 vs	Metal-metal vibrations
	118 s			118 s		Polar vibrations Rb-O
	135 s					Translational modes Rb
			138 s	138 sh	138 s	Displacement of octahedra
143 s		143 s				to respect de matrix
			158 m	158 m	158 m	
160 m	160 m	160 m				
	171 s	171 vs		171 sh		
	202 st			202 st		ν_6 TiO_6
			205 st		205 st	
211 st		211 st				
	215 s					
				224 m		
228 s	228 m	228 sh				
	265 st		265 st	265 st	265 vst	ν_5 TiO_6
270 st		270 vst				
285 st	285 s	285 st	285 st	285 sh	285 st	
297 s		297 vs	297 sh			
		304 vs				
311 s	311 m		311 vs	311 m		ν_4 TiO_6
329 s	329 st	329 s	329 s	329 st	329 vs	
		362 st			362 st	Octahedra sharing corners
			368 st	368 m		
370 st	370 m					
395 m	395 s	395 st	395 m	395 s	395 st	ν_2 PO_4
	406 s		406 vs	406 s		
415 vs	415 s		415 vs	415 s		
		423 s			423 s	
465 s	465 s	465 s	465 s	465 s	465 s	ν_4 PO_4
519 m	519 vs					
			523 m	523 vs		
549 s	549 vs		549 s		549 vs	
				556 s		
	558 s					
	567 s					
574 vs			574 vs			
			594 s	594 vs	594 sh	
598 s	598 s					
			618 m		618 m	ν_2 TiO_6
621 s		621 m				
				627 m		
	631 m					
			647 sh		647 sh	

688 vst		688 vst	688 vst		688 vst	
				691 vst		ν_1 and ν_3 TiO_6
	694 vst					
			788 sh	788 sh	788 sh	
833 s	833 s	833 s	833 s	833 s	833 s	Nb-O-Ti vibration
	958 s			958 s		ν_1 PO_4
966 s	966 vs	966 s	966 m	966 vs	966 vs	
984 vs	984 vs	984 s	984 s			
					987 vs	
	997 vs			997 vs		
	1025 s			1025 vs		
1037 s		1037 s				
			1040 m		1040 s	
1091 s	1091 m		1091 m	1091 vs		
	1114 vs			1114 vs		
						ν_3 PO_4

Table 6.5. *Raman bands observed in $RbTi_{1-x}Nb_xOPO_4$ (x = 0 and 0.06) at room temperature for the $y(xx)\bar{y}$, $y(xz)\bar{y}$, $y(zz)\bar{y}$ configurations.*

$RbTiOPO_4$			**$RbTi_{0.94}Nb_{0.06}OPO_4$**			**Assignation**
$y(xx)\bar{y}$	$y(xz)\bar{y}$	$y(zz)\bar{y}$	$y(xx)\bar{y}$	$y(xz)\bar{y}$	$y(zz)\bar{y}$	
					46 s	
		49 s				
				50 s		
	54 s					
		61 s				
		66 s			66 s	
81 vs	81 vs	81 s	81 vs		81 s	Polar vibrations Rb-O
			92 s	92 s	92 s	
96 s		96 s				
	99 s					
104 s		104 m	104 m	104 m	104 m	Metal-metal vibrations
				125 s		Polar vibrations Rb-O
			137 s	137 s	137 m	Translational modes Rb^+
142 s	142 s	142 m				
			157 s	157 s	157 m	Displacement of the
	159 s	159 m				octahedra to respect the
		169 s				matrix
	178 s			178 m		
				183 m		
	188 s					
204 vs	204 vs		204 m	204 m	204 st	ν_6 TiO_6
210 s	210 s	210 vst				
	256 s			256 s		
262 s						ν_5 TiO_6
			266 s	266 m	266 vst	
269 s	269 m	269 vst				
279 s		279 vst	279 s			
	284 m	284 vst				
				286 m	286 vst	
	294 m					
296 s		296 m				
			299 s		299 sh	
303 s		303 m				
317 vs	317 m	317 s	317 vs	317 m		ν_4 TiO_6
	344 m		344 m			Polar vibrations Rb-O

361 s	361 s	361 vst	361 s	361 s	361 vst	
394 s	394 s	394 vst	394 s	394 s	394 vst	ν_2 PO_4
	402 s					
422 st	422 m	422 st	422 st	422 m	422 st	
		463 s				
					465 s	
476 s						
			478 s			
	490 s	490 s		490 s		ν_4 PO_4
518 s						
			522 m	522 s	522 s	
			547 s		547 s	
549 s		549 s				
	557 s					
				561 s		
	593 s	593 s		593 s	593 s	
			616 s	616 s	616 st	ν_2 TiO_6
620 s	620 s	620 st				
	633 s			633 s		
687 st	687 m	687 vst	687 st	687 mt	687 vst	ν_1 and ν_3 TiO_6
731 s	731 s					
	781 m		781 vs	781 s	781 sh	
			832 s		832 s	ν_1 PO_4
			965 s	965 s	965 s	
	968 s					
983 s		983 s				
			985 s		985 s	
	987 s			987 s		
	996 s			996 s		
1036 s	1036 s	1036 m				
			1039 s	1039 s	1039 m	
				1090 s	1090 vs	ν_3 PO_4

Table 6.6. *Raman bands observed in $RbTi_{1-x}Nb_xOPO_4$ (x = 0 and 0.06) at room temperature for the $z(xx)\bar{z}$, $z(xy)\bar{z}$, $z(yy)\bar{z}$ configurations.*

$RbTiOPO_4$			**$RbTi_{0.94}Nb_{0.06}OPO_4$**			**Assignation**
$z(xx)\bar{z}$	$z(xy)\bar{z}$	$z(yy)\bar{z}$	$z(xx)\bar{z}$	$z(xy)\bar{z}$	$z(yy)\bar{z}$	
49 m	49 m	49 m				
			51 m	51 m	51 m	
60 s	60 s	60 m			60 m	
			67 m	67 m	67 m	
73 m	73 s	73 s	73 s			
80 st	80 s		80 m			Polar vibrations Rb-O
95 m			95 m			
104 st	104 st	104 m	104 st	104 st	104 m	Metal-metal vibrations
		109 m				Displacement of the
					111 m	octahedra in relation to the
	118 m					matrix
				120 m		Polar vibrations Rb-O
				133 s		
	135 m					
142 m		142 m	142 m		142 s	
161 s	161 m	161 st	161 s	161 m	161 st	
		171 sh				
	190 m			190 m		
203 sh		203 sh			203 sh	ν_6 TiO_6
211 m	211 s	211 st	211 m	211 s	211 st	

	224 vs	224 s				
			232 vs	232 s		
		238 m			238 m	
	258 s					
262 s		262 m	262 s		262 m	ν_5 TiO_6
	265 s				265 st	
		277 m			277 st	
281 m			281 st			
	283 m					
				285 st		
298 m	298 m	298 st	298 m	298 m	298 st	
313 m	313 m	313 st	313 m	313 m	313 st	ν_4 TiO_6
		330 m			330 m	
334 m	334 st	334 m				Polar vibrations Rb-O
			337 m	337 st		
345 s	345 st					
			347 s	347 st		
367 m	367 s	367 st	367 m	367 m	367 vst	ν_2 PO_4
393 m	393 s	393 st	393 m	393 s	393 st	
					414 m	
417 st	417 s	417 s				
			419 s	419 s		
437 s						
476 st	476 vs	476 sh				
			480 st	480 s	480 sh	ν_4 PO_4
490 m	490 s	490 st			490 st	
518 st	518 s	518 st				
			523 st	523 m	523 st	
549 st	549 s	549 st	549 st	549 s	549 st	
		573 s			573 m	
587 s		587 s	587 m		587 sh	
		597 s	597 s	597 vs	597 m	
627 m	627 vs	627 m	627 m	627 s	627 m	ν_2 TiO_6
	693 s	693 m		693 m	693 st	
761 m	761 st	761 vst	761 m	761 st	761 vst	
	794 st					
				796 st		
	816 st					
833 m	833 vs	833 st	833 m	833 vs	833 st	ν_1 PO_4
957 vs	957 s					
		965 st			965 st	
	968 m			968 m		
978 st	978 s	978 m				
			980 st			
	994 s					
				996 s		
1006 m		1006 m				
			1011 m		1011 m	
					1023 s	
	1080 vs	1080 st		1080 s	1080 st	ν_3 PO_4
1115 s		1115 m				
			1117 s		1117 m	

6.4. The Non-Linear Optical properties of $RbTiOPO_4$:Nb crystals.

SHG efficiency analysed by the powder method of Kurtz et al.,[150] which is defined as the relationship between the powers of the pumping beam (1064 nm) and the green beam (532 nm), and

measured in $RbTi_{1-x}Nb_xOPO_4$ (x = 0, 0.02, 0.04, 0.05 and 0.07) is shown in Table 5 in *paper V*. The SHG efficiency of RTP was slightly lower than that of KTP, which we expected from previous reports.[174] Partially substituting Ti with Nb increases the SHG efficiency of RTP to that of KTP. This efficiency reaches a maximum for a substitution of Ti by Nb of around 4-5 atom %. For higher concentrations of Nb, the SHG efficiency decreases and when the concentration of Nb substituting Ti in the crystals is around 7 atom %, SHG efficiency is similar to that with undoped RTP.

We also measured the fundamental wavelength of type II angular non-critical phase-matching (NCPM) for second harmonic generation in single crystals of $RbTi_{1-x}Nb_xOPO_4$ (x = 0 and 0.06) in the *x-z* and *y-z* planes. Table 6.7 summarises the experimental NCPM wavelengths obtained for RTP and RTP:Nb. For purposes of comparison, the table includes the values of KTP.[223]

Phase-matching is impossible for wavelengths that are smaller than the one that leads to NCPM along the *y*-axis. These results show that while RTP does not allow type II phase-matching below about 1 μm, the presence of Nb in the crystals shifts the fundamental wavelength for NCPM interactions to below those obtained in RTP along the *x* and *y* axis, and that the shift to shorter wavelengths is greater in the *y* direction. The fundamental wavelength for NCPM interactions in the *y* direction is even shorter than that with KTP (SHG is possible below 994 nm).

Table 6.7. *Fundamental wavelengths of type II angular non-critical phase-matching interactions for SHG in $RbTi_{1-x}Nb_xOPO_4$ (x = 0 and 0.06) in the x-z and y-z planes and their comparison with those of KTP.*

Crystal	**Fundamental wavelengths of type II NCPM interactions (nm)**	
	x-z plain	*y-z* plain
RTP	1139	1030
RTP:Nb	1094	979
KTP	1079	994

Initial Page **Table of Contents**